

Article

Synthesis of Ti-Cu Multiphase Alloy by Spark Plasma Sintering: Mechanical and Corrosion Properties

Oleg O. Shichalin ^{1,*}, Vladimir N. Sakhnevich ¹, Igor Yu. Buravlev ¹, Aleksey O. Lembikov ¹, Anastasia A. Buravleva ¹, Semen A. Azon ¹, Sofia B. Yarusova ^{2,3}, Sakhayana N. Danilova ⁴, Alexander N. Fedorets ¹, Anton A. Belov ¹ and Evgeniy K. Papynov ¹

- ¹ Nuclear Technology Laboratory, Department of Nuclear Technology, Institute of High Technologies and Advanced Materials, Far Eastern Federal University, 690922 Vladivostok, Russia; sakhnevich.vn@students.dvfu.ru (V.N.S.); buravlev.i@gmail.com (I.Y.B.); lembikov.ao@students.dvfu.ru (A.O.L.); bouy@mail.ru (A.A.B.); azon.sa@dvfu.ru (S.A.A.); fedorec.an@dvfu.ru (A.N.F.); nefryty@gmail.com (A.A.B.); papynov@mail.ru (E.K.P.)
- ² Laboratory of Protective Coatings and Marine Corrosion, Institute of Chemistry, Far Eastern Branch, Russian Academy of Sciences, 690022 Vladivostok, Russia; yarusova_10@mail.ru
- ³ Basic Department of Ecology and Ecological Problems of Chemical Technology, Vladivostok State University of Economics and Service, 690014 Vladivostok, Russia
- ⁴ Department of Chemistry, Institute of Natural Sciences, North-Eastern Federal University, 677000 Yakutsk, Russia; dsn.sakhayana@mail.ru
- * Correspondence: oleg_shich@mail.ru



Citation: Shichalin, O.O.; Sakhnevich, V.N.; Buravlev, I.Y.; Lembikov, A.O.; Buravleva, A.A.; Azon, S.A.; Yarusova, S.B.; Danilova, S.N.; Fedorets, A.N.; Belov, A.A.; et al. Synthesis of Ti-Cu Multiphase Alloy by Spark Plasma Sintering: Mechanical and Corrosion Properties. *Metals* **2022**, *12*, 1089. <https://doi.org/10.3390/met12071089>

Academic Editors: Taekyung Lee and Jong-Taek Yeom

Received: 25 May 2022

Accepted: 23 June 2022

Published: 25 June 2022

Publisher's Note: MDPI stays neutral with regard to jurisdictional claims in published maps and institutional affiliations.



Copyright: © 2022 by the authors. Licensee MDPI, Basel, Switzerland. This article is an open access article distributed under the terms and conditions of the Creative Commons Attribution (CC BY) license (<https://creativecommons.org/licenses/by/4.0/>).

Abstract: To study the material based on the binary system Ti + Cu (50% atm), samples were produced from powders of commercially pure metals and additionally ground in a ball mill (final size about 12 μm) by spark plasma sintering. The following intermetallic phases were obtained in the materials: CuTi₂, TiCu, and Ti₃Cu₄. The materials have a hardness of 363 and 385 HV (800 and 900 °C), a microhardness of 393 and 397 μHV, a density of 4.24 and 5.23 kg/m³, and resistance to corrosion in acids (weight gain + 0.002% after 24 h of testing according to ISO 16151 for a sample with 900 °C—the best result in comparison with steel 308, AA2024, CuAl₁₀Fe₃Mn₂). The hardness value varies due to the presence of pure metal agglomerates. The relationship between the temperature of spark plasma sintering and the characteristics of the material (material parameters improve with increasing temperature, segregation is reduced) is revealed.

Keywords: intermetallics; titanium; copper; spark plasma sintering (SPS)

1. Introduction

Scientific and technological progress is based on modern scientific and technological solutions, which result in modern high technology and new generation materials (functional materials). On their basis, the creation of competitive innovative products or the formation of large-scale more efficient production facilities that bring any industrial sector to a new modern level is ensured. For example, in recent decades, the market of modern materials with special properties has been actively formed, which include super hard materials [1], materials with a shape memory effect [2], materials with superfluidity [3] and superconductivity [4], corrosion-resistant materials [5,6], etc. The need for modern materials can be satisfied by intermetallic compounds, the number of studies on which has increased significantly in recent years [7,8].

Intermetallic compounds are commonly referred to as materials that are an ordered solid compound between two or more metallic elements. Intermetallic compounds, as a rule, are characterized by relatively high hardness, but at the same time they are brittle. Additionally, they actively used for high-temperature environment (metallic properties appears closer to melting point) [9,10].

High-entropy [11] or porous [12] and classical binary compounds [13–15] are widely known. Of particular interest are alloys such as nitinol, which have shape memory, high hardness, and excellent anticorrosion properties [15]. Materials based on titanium-copper have the potential to have some properties like this.

Forming a Ti_2Cu compound with titanium, copper lowers the combustion rate at high temperatures [16], the substance acts as a thermal barrier. Materials with fcc and hcp (copper and titanium) lattices tend to harden under the influence of low temperatures, experience local martensitic transformation. Intermetallic compounds have high strength and hardness. It was also noticed that with an increase in the copper content in titanium (flesh up to 74 atomic%), wear resistance and hardness increase [17]. All these qualities make it possible to admit the possibility of the appearance of a material based on Cu-Ti with good performance properties.

Due to the large difference in melting temperatures and densities, it is impossible to obtain titanium and copper alloys by classical methods (melt mixing). From the scientific literature, methods are known for obtaining intermetallic material by high-temperature pressing [18,19], reactive sintering [20], magnetron sputtering [6], electrospark deposition [21], reduction in salts (reduction of Ti-Al in $CaCl_2$ using sodium) [22], arc melting [17], and spark plasma sintering.

The latter method makes it possible to produce compounds of almost any metallic composition [1,23,24]. The established advantages of SPS over traditional technologies are as follows: (a) low sintering temperatures, (b) short sintering cycle times (minutes), (c) low power consumption (about 1/5 of HP), (d) uniform heating of the material, (e) control of the temperature gradient, (f) absence of sintering additives and plasticizers, (g) sintering of powders with a wide particle size distribution, (h) achieving maximum density of the material (up to 100% of theoretical), (i) one-stage sintering, and (j) cleaning of the particle surface under the influence of current. In addition, high-speed heating ensures the formation of unique physical and chemical characteristics and properties of the resulting materials. Synthesis of materials is possible with the preservation of the initial grain size and microstructure, the formation of various porosities, and the achievement of high density and structural strength of compacts. The synthesis of metastable materials with the preservation of this state is provided. The control of phase transformations is achieved by eliminating or initiating solid-phase chemical interactions during material processing [25–32].

Previously, successful experiments have already been carried out to obtain Ti-Cu systems, which resulted in samples with a non-uniform phase composition [33,34]. An interesting feature of these experiments is the presence of the $CuTi_2$ phase almost independently of the Cu content in the material.

This work is aimed at studying the properties of a material based on titanium and copper (50×50 atm%) obtained by spark plasma sintering. Identification of the relationship between sintering temperature and mechanical, physical properties, and corrosion resistance. At the moment, the material properties of alloys having equal atomic number of Ti and Cu have not yet been investigated.

2. Materials and Methods

2.1. Materials

For the manufacture of starting mixed compositions (starting powders), grade Ti and Cu powders with a purity of 99.9% were used.

The scheme of experiment is shown in Figure 1. The test chosen was a hardness test not only in HV, but also in μHV , because the samples are multiphase and have different values in different areas of the surface.

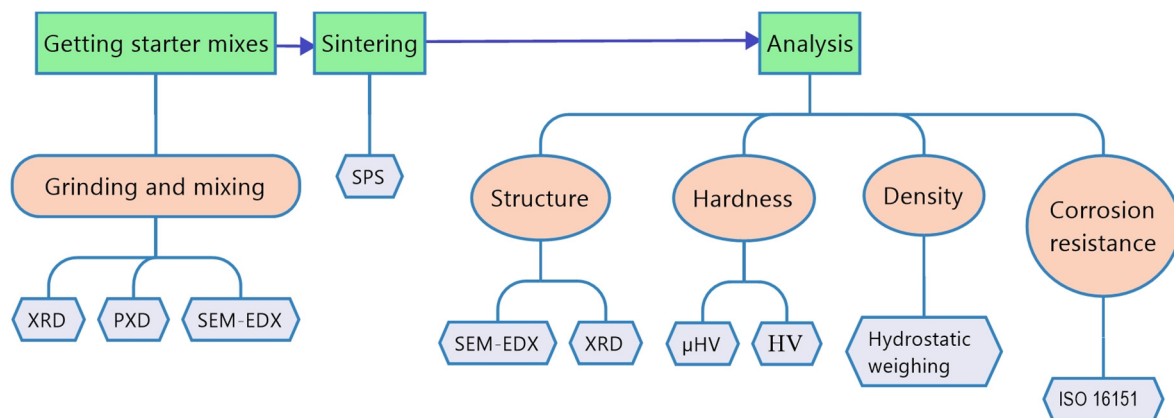


Figure 1. Scheme of the experiment.

2.2. Powder Prepare

Grinding was carried out in a ball mill in argon atmosphere at a frequency of 700 rpm for 5 h in a Tencan XQM-0.4A vertical planetary ball mill (China). The parameters of the mixing process with simultaneous grinding are presented in Table 1. The results of SEM images are shown in Figure 1. Part of the obtained powder was isostatically pressed into a press-SJYP-12TS, at a pressure of 20 MPa (8000 kg). In this way, tablets with a diameter of 10 mm and a height of 5–7 mm were obtained.

Table 1. Contents of mixing beakers.

Weight of Titanium Powder, g	28.56	Dimension	60–70 μm
Weight of Copper Powder, g	21.46	Dimension	40–60 μm
Weight of Grinding Balls, g	75	Dimension	10 and 5 mm in a diameter
Grinding Ball Material	WC		

2.3. Powder Sintering

Consolidation was carried out by the method of spark plasma sintering at the SPS-515S (Dr. Sinter LABTM, Kyoto, Japan), at temperatures of 800 and 900 °C under a pressing pressure of 50 MPa, with a holding time of 5 min. The temperature of the SPS process was controlled by an optical pyrometer IR-AHS (Hitachi, Tokyo, Japan), focused on a hole located in the middle of the plane of the outer wall of the mold, 5.5 mm deep. The sintered material was heated with a unipolar pulsed current with forced low-voltage pulses in the on/off mode in 12/2 bursts (pulse burst duration 39.6 ms/pause 6.6 ms). The maximum current during sintering was 600 A, and the voltage was 4 V.

Characterization of Analytical and Physical Methods

The change in the granulometric composition of the initial powders during mechanical mixing with grinding at different process times (with an increase in the number of cycles) was analyzed on an Analysette-22 NanoTec/MicroTec/XT laser particle analyzer (Fritsch, Munich, Germany); for each sample, measurements were carried out 3 times, then the results were averaged. The elemental composition was determined by energy dispersive X-ray fluorescence on a EDX 7000 HS instrument (Shimadzu, Tokyo, Japan). The microstructure features were studied on an ECLIPSE MA200 metallographic microscope and a scanning electron microscope (SEM) (Nikon, Düsseldorf, Germany). The average grain size was determined from the HAADF-STEM images, in accordance with ASTM E112-110. Vickers hardness was measured in accordance with ISO 6507-1:2018. Microhardness was measured with a load of 0.98 N using an HMV-G-FA-D automatic microhardness tester (Shimadzu, Tokyo, Japan).

3. Results and Discussion

3.1. Preparation of Starter Mixtures

The effect of the grinding process on the powders is shown in Figure 2; before treatment, the Ti and Cu powders had an average particle size of 40–70 μm .

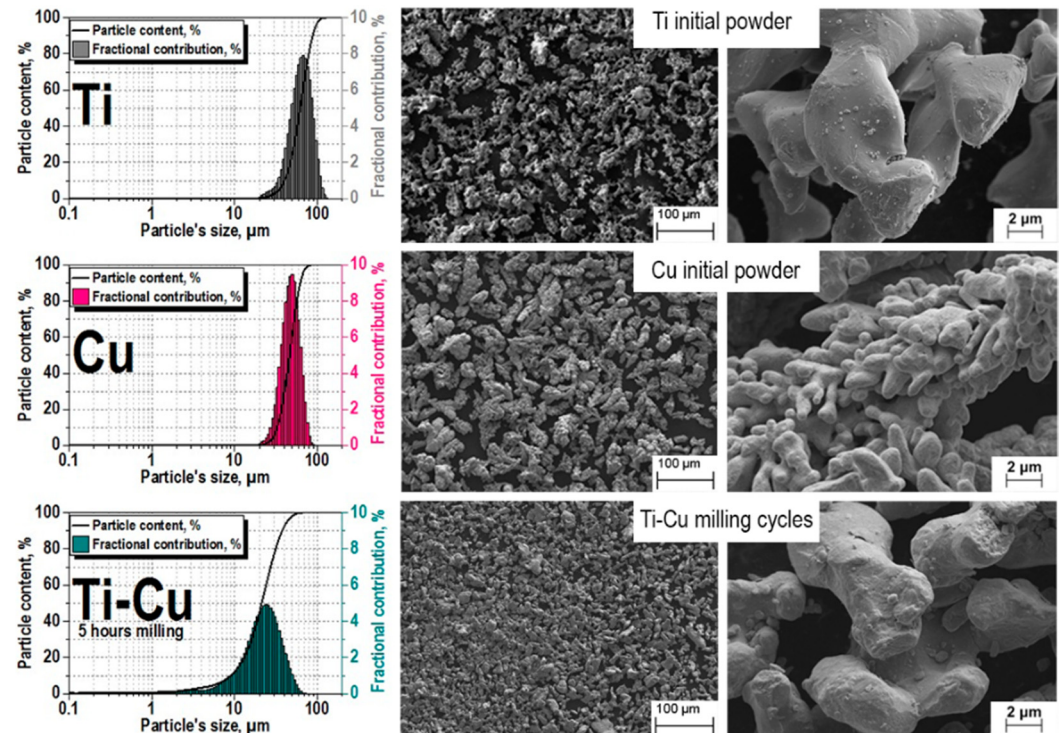


Figure 2. Powder particle sizes before and after grinding.

It can be seen from the image above that, as a result of grinding, the average value of the particle size became equal to 20–30 microns and compaction occurred, which is actively promoted by the final bean-shaped shape of the particles. The somewhat greater roughness is the result of partial oxidation because of grinding (argon atmosphere include trivial part of oxygen). The mixture is ready for pressing.

3.2. Synthesis of Alloys of the Ti-Cu System

The diffraction pattern of the sample sintered at 800 $^{\circ}\text{C}$ and 900 $^{\circ}\text{C}$, respectively, contains CuTi_2 , CuTi , Cu , and Ti phases (Figures 3 and 4). The sample sintered at 800 $^{\circ}\text{C}$ also has a Cu_4Ti_3 phase. The diffraction patterns of CuTi_2 and CuTi_3 are similar, the CuTi_2 phase is confirmed specifically by the fact that there is a characteristic reflection for this phase at 16.5 2 theta, and there is no characteristic reflection at 21.4 2 Theta for the CuTi_3 phase. Refinement by the Rietveld method was carried out in the program “Topas”; the R-factor of samples sintered at 800 $^{\circ}\text{C}$ and 900 $^{\circ}\text{C}$ does not exceed 4%. The results of the refinements are attached in Table 2.

Content of the CuTi_2 phase increases with increasing temperature. It has been established that the population of titanium in the crystal lattice is higher than that of copper. The conversion from mass fractions to molar fractions, taking into account the population, indicated that the ratio of Titanium to Copper in the mixture is 1 to 0.8. The discrepancy between the mole fractions is explained by the fact that the filming takes place from the surface of the material. The CuTi_2 phase is also proved by the fact that, when the population is refined and converted into mole fractions, the ratio of titanium to copper is 2 to 1, which can no longer be explained by the error. According to the results of the refinement of the lattice parameters, it was found that with an increase in the sintering time, the lattice

parameters increase, which indicates a decrease in the density of the sample. Some of lattice parameters are given in Table 3.

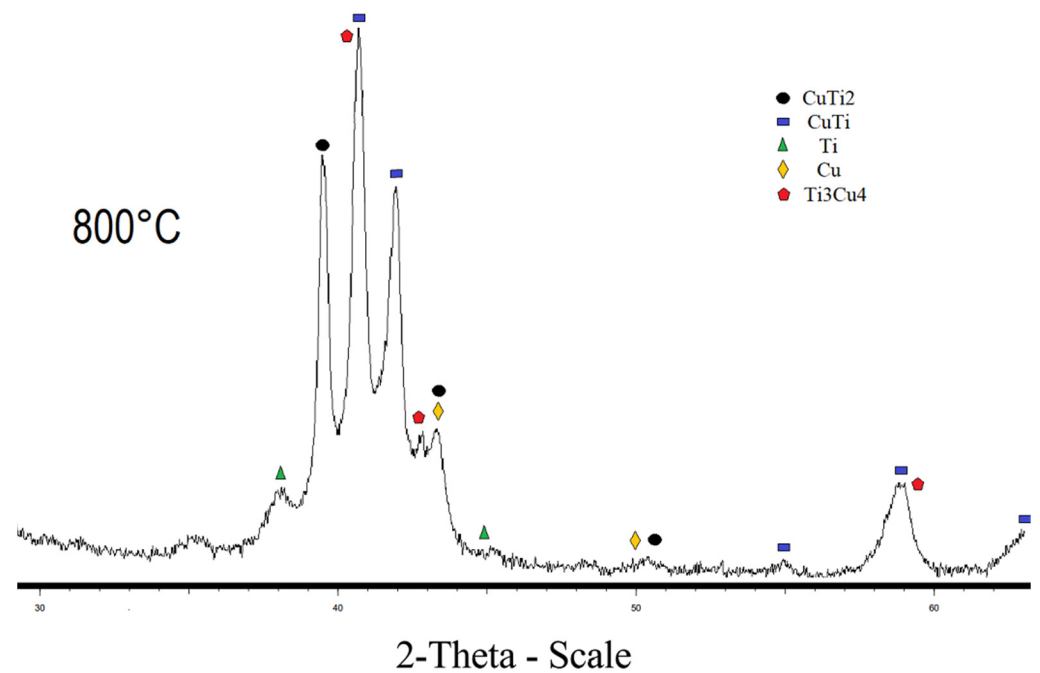


Figure 3. X-ray pattern of specimen obtained at 800 °C.

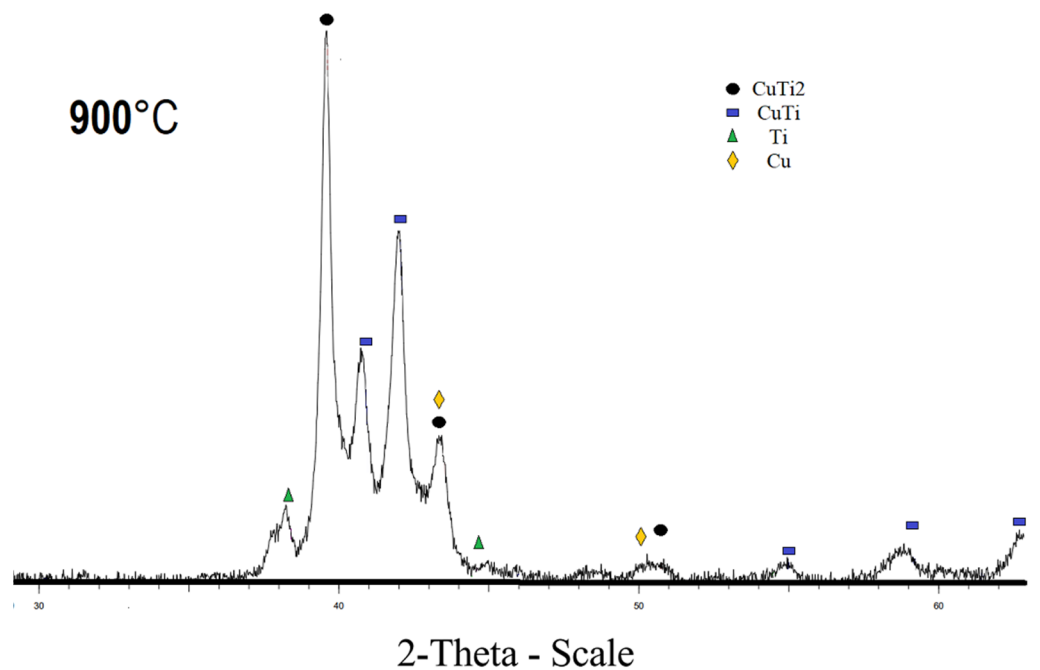


Figure 4. X-ray pattern of specimen obtained at 900 °C.

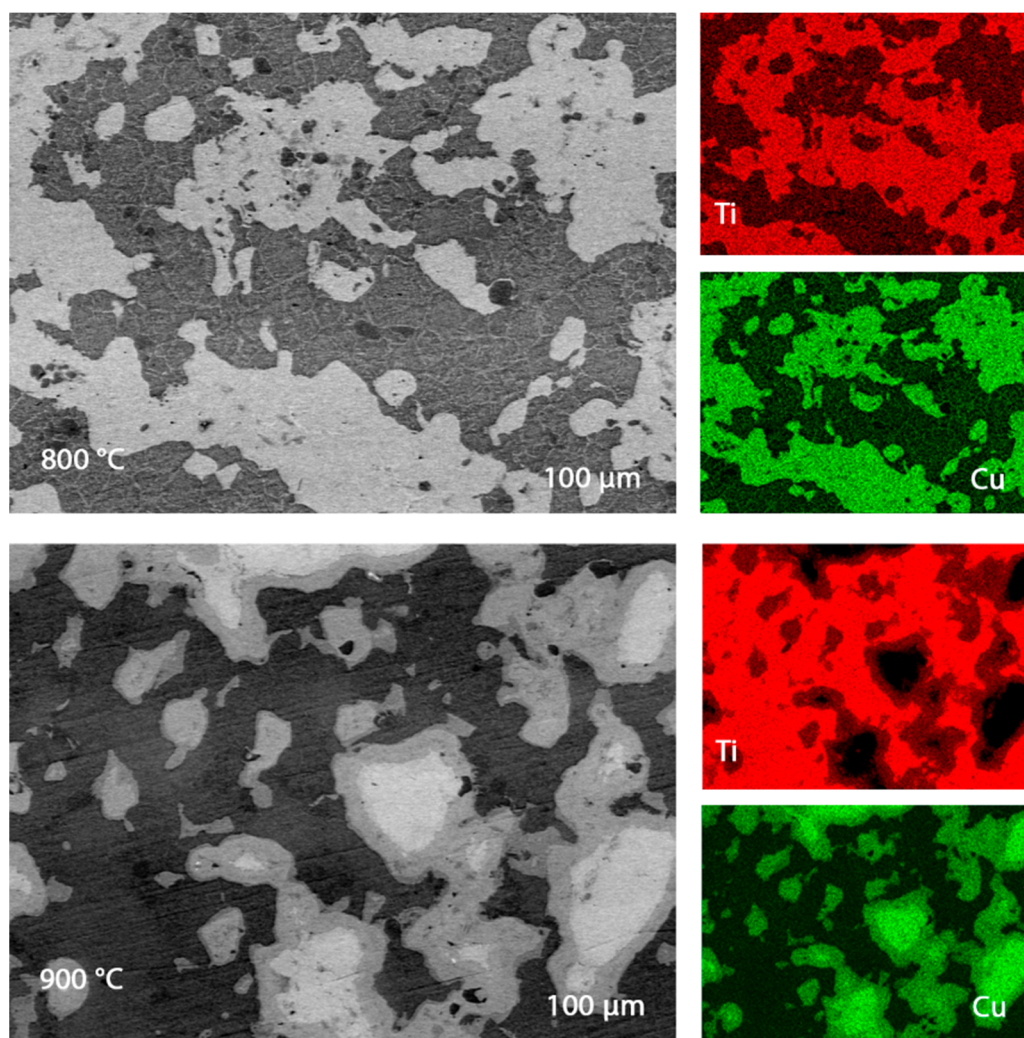
Table 2. Weight configuration of specimens.

T of Sintering, °C	wt.%, TiCu	wt.%, CuTi ₂	wt.%, Ti ₃ Cu ₄	wt.%, Ti	wt.%, Cu
800	53	28	9	5	5
900	45	46	-	5	4

Table 3. Crystallography parameters of specimens.

Lattice Parameters, Å		800 °C	Theoretical Density		900 °C	Theoretical Density
CuTi	a.	3.12555	6372 kg/m ³	a.	3.13719	6345 kg/m ³
	b.	3.12555		b.	3.13719	
	c.	2.96124		c.	2.96540	
CuTi ₂	a.	2.94417	5696 kg/m ³	a.	2.95297	5616 kg/m ³
	b.	2.94417		b.	2.95297	
	c.	10.7551		c.	10.7698	

Scanning electron microscope images of polished ends are shown in Figure 5, where the impurity content was no more than Cr—0.83%, P—0.52%, Si—0.16%, and Al—0.16%. The ubiquitous location of pure metals makes the material a kind of composite, which should have an unusual effect on its corrosion resistance and microhardness. The grain size of the samples obtained in the current experiment is about 7 μm , which is larger than the values of the samples from the works of Rui Dong, Weiwei Zhu, and others, when the synthesis was received at 750 °C. This fact also explains the lower hardness values (about 453 HV vs. 393 HV in our experiment) [33]. Comparing these experiments, we can conclude that an increase in temperature can cause the growth of grains of pure metals, which adversely affects the hardness.

**Figure 5.** Electronic images of the sample plane, titanium, and copper content.

3.3. Physical and Mechanical Properties of Samples

The established microhardness of samples sintered in plasma is at the level of 393 HV, with increasing temperature, the hardness increases only slightly (Figure 6), in both samples there are readings much lower than the average, which indicates the presence of pure phase metals. Vickers hardness measurements showed similar values (363 and 385 HV for samples sintered at 800 and 900 °C, respectively), which is a good indicator of hardness for non-ferrous alloys (values usually up to 320 HV) [35,36]. However, it should be noted that the samples obtained by arc melting have higher hardness values, and they are also multiphase [17]. Based on the results of the images of the sample, one can judge the sufficient plasticity of the sample (the absence of cracks from the pyramidal imprint) (Figure 7).

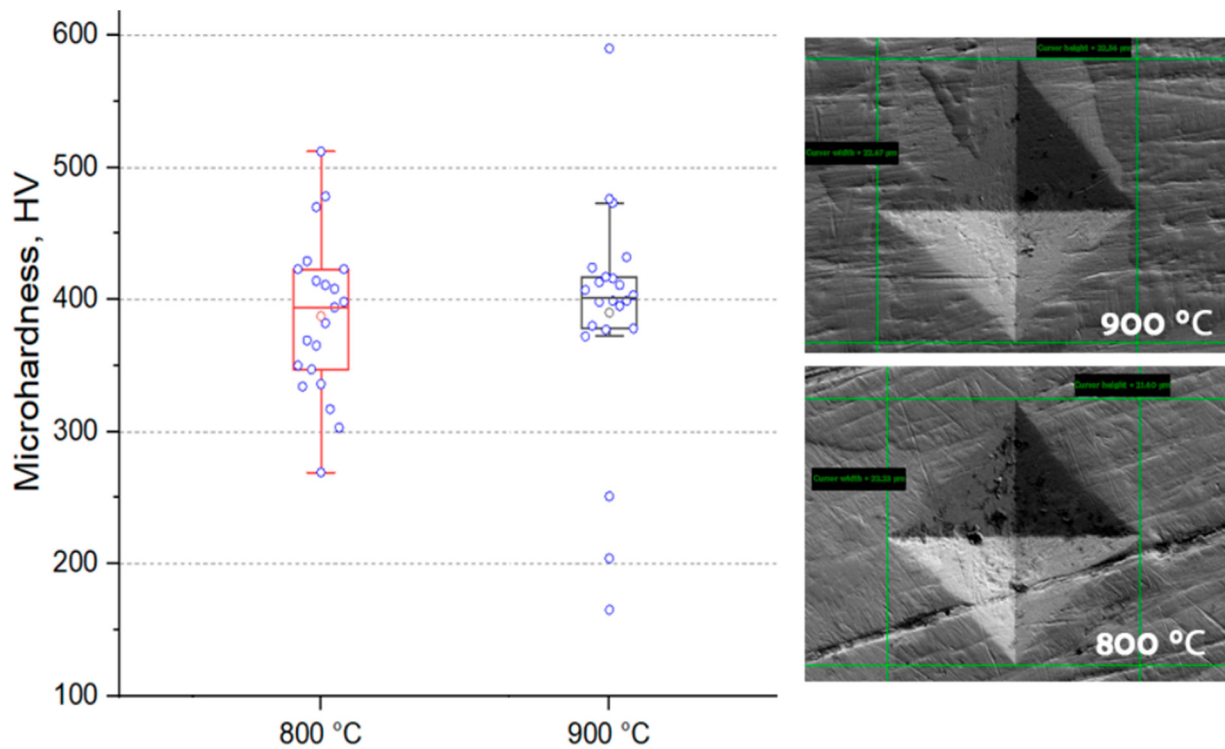


Figure 6. Microhardness value for materials obtained by spark plasma sintering.

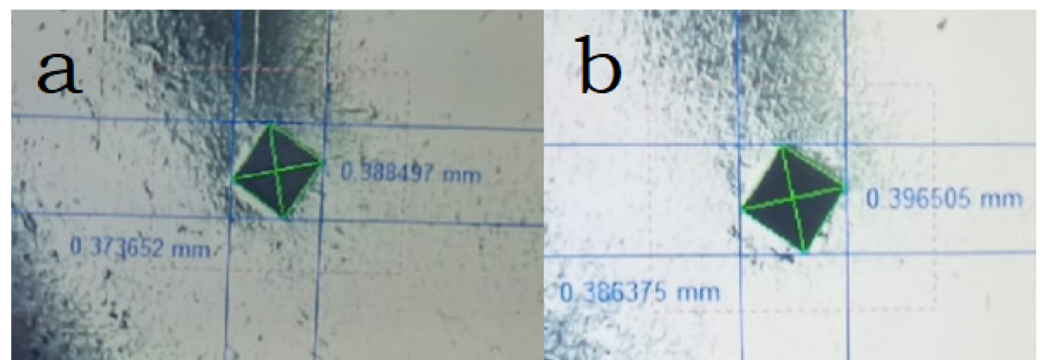


Figure 7. Imprint of the hardness tester indenter of samples sintered at different temperatures: (a) 900 °C, (b) 800 °C.

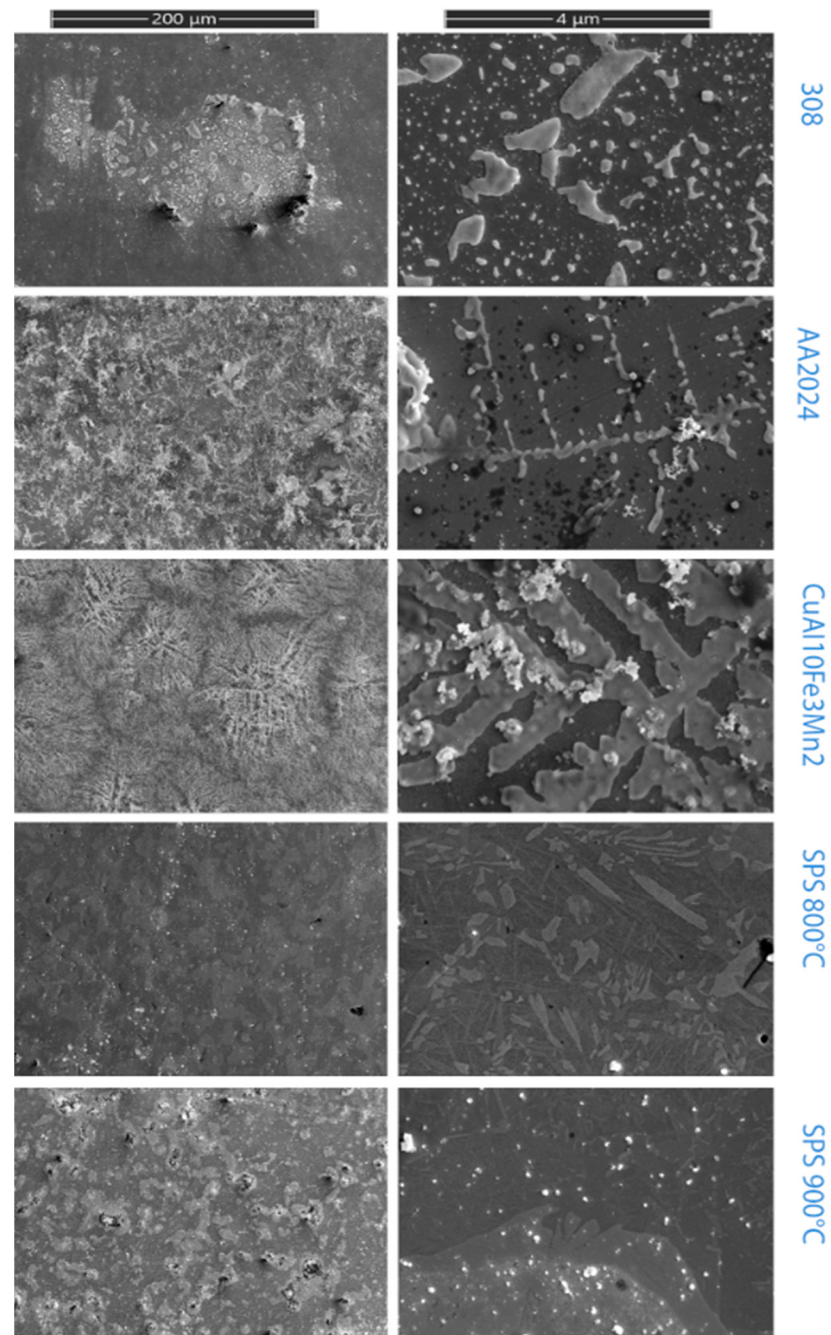
Table 4 shows the main parameters of the two samples and their preparation.

Table 4. Parameters of the studied samples and their preparation.

T, °C	P, MPa	t, min	μHV	HV	ρ, kg/m ³
800	50	5	393	363	4540
900	50	5	397	385	5230

3.4. Corrosion Resistance of Material

For comparison, within 24 h, along with the material, samples of stainless steel, duralumin, and corrosion-resistant bronze were also exposed to aggressive media. Figure 8 shows images of the surfaces of samples subjected to testing of corrosive environments; Table 1 shows the change in the mass of samples.

**Figure 8.** Samples after corrosion testing.

The test was carried out according to ISO 16,151 (sodium chloride + sulfuric acid + nitric acid) [37]. As can be seen from the Table 5, the experimental sample obtained at 900 °C has the least tendency to corrosion, close to stainless steel. The experimental sample with a sintering temperature of 800 °C has the largest weight gain, which is mainly associated with the presence of micropores, which are clearly visible on the etched sample. The presence of the Cu₄Ti₃ phase content also does not impart corrosion resistance in comparison with a large amount of the CuTi₂ phase. The most corrosion-resistant sample contains a lot of CuTi₂ phase and does not contain phase Cu₄Ti₃. This confirms the importance of this phase for corrosion resistance [16]. Pure copper present in the metal shows less corrosivity due to the presence of titanium in general.

Table 5. Influence of being in a corrosive environment on the mass of metal samples.

308	AA2024	CuA110Fe ₃ Mn ₂	SPS 800 °C	SPS 900 °C
+0.006	+0.022	−0.03	+0.137	−0.002

4. Conclusions

The work demonstrates the potential of alloys of binary titanium-copper compounds, where samples containing many phases have high hardness, low density, and corrosion resistance. The combination of good mechanical properties of multiphase alloys obtained in this work suggests the idea of further research of such materials. Like high-entropy alloys, the multiphase system can exhibit high mechanical properties. The work also led to several important findings related to the Ti-Cu system:

- Spark plasma sintering helps to obtain samples with high hardness for non-ferrous alloys (≈ 395 HV), low density, and resistance to acids.
- As the temperature of spark plasma sintering increases, the phase composition changes and the mechanical properties increase, and compaction can be associated both with specific phases and with an increase in pressure from thermal expansion.
- The presence of phase Cu₄Ti₃ in the sample sintered at 800 °C does not provide high corrosion protection, so phase B is preferable for a material used in an aggressive environment.

Author Contributions: Conceptualization, O.O.S.; Data curation, I.Y.B. and S.A.A.; Formal analysis, O.O.S.; Investigation, V.N.S., A.O.L., A.A.B. (Anastasia A. Buravleva) and A.A.B. (Anton A. Belov); Methodology, A.N.F.; Resources, S.B.Y. and S.N.D.; Supervision, E.K.P.; Writing—original draft, O.O.S. All authors have read and agreed to the published version of the manuscript.

Funding: The synthesis and characterization of the metal samples were funded by the State Assignment of the Ministry of Science and Higher Education of the Russian Federation No. 00657-2020-0006. (E.K. Papynov—project Manager).

Institutional Review Board Statement: Not applicable.

Informed Consent Statement: Not applicable.

Data Availability Statement: Not applicable.

Conflicts of Interest: The authors declare no conflict of interest.

References

1. Shichalin, O.O.; Buravlev, I.Y.; Papynov, E.K.; Golub, A.V.; Belov, A.A.; Buravlev, A.A.; Sakhnevich, V.N.; Dvornik, M.I.; Vlasovac, N.M.; Gerasimenko, A.V.; et al. Comparative study of WC-based hard alloys fabrication via spark plasma sintering using Co, Fe, Ni, Cr, and Ti binders. *Int. J. Refract. Met. Hard Mater.* **2022**, *102*, 105725. [CrossRef]
2. Alagha, A.N.; Hussain, S.; Zaki, W. Additive manufacturing of shape memory alloys: A review with emphasis on powder bed systems. *Mater. Des.* **2021**, *204*, 109654. [CrossRef]
3. Xiang, T.; Chen, D.; Lv, Z.; Yang, Z.; Yang, L.; Li, C. Robust superhydrophobic coating with superior corrosion resistance. *J. Alloys Compd.* **2019**, *798*, 320–325. [CrossRef]
4. Conti, S.; Neilson, D.; Peeters, F.M.; Perali, A. Transition metal dichalcogenides as strategy for high temperature electron-hole superfluidity. *Condens. Matter* **2020**, *5*, 22. [CrossRef]

5. Zhou, S.; Zhao, Y.; Wang, X.; Li, W.; Chen, D.; Sercombe, T.B. Enhanced corrosion resistance of Ti-5 wt.% TiN composite compared to commercial pure Ti produced by selective laser melting in HCl solution. *J. Alloys Compd.* **2020**, *820*, 153422. [[CrossRef](#)]
6. Lopes, C.; Gabor, C.; Cristea, D.; Costa, R.; Domingues, R.P.; Rodrigues, M.S.; Borges, J.; Alves, E.; Barradas, N.P.; Munteanu, D.; et al. Evolution of the mechanical properties of Ti-based intermetallic thin films doped with different metals to be used as biomedical devices. *Appl. Surf. Sci.* **2020**, *505*, 144617. [[CrossRef](#)]
7. Rößner, L.; Armbrüster, M. Electrochemical Energy Conversion on Intermetallic Compounds: A Review. *ACS Catal.* **2019**, *9*, 2018–2062. [[CrossRef](#)]
8. Armbrüster, M. Intermetallic compounds in catalysis—a versatile class of materials meets interesting challenges. *Sci. Technol. Adv. Mater.* **2020**, *21*, 303–322. [[CrossRef](#)] [[PubMed](#)]
9. Askeland, D.R. *The Science and Engineering of Materials*; Springer: Boston, MA, USA, 1996; pp. 414–417.
10. Soboyejo, W. *Mechanical Properties of Engineered Materials*; CRC Press: Boca Raton, FL, USA, 2002; pp. 385–387.
11. Yao, K.; Liu, L.; Ren, J.; Guo, Y.; Liu, Y.; Cao, Y.; Feng, R.; Wu, F.; Qi, J.; Luo, J.; et al. High-entropy intermetallic compound with ultra-high strength and thermal stability. *Scr. Mater.* **2021**, *194*, 113674. [[CrossRef](#)]
12. Jiang, Y.; He, Y.; Gao, H. Recent progress in porous intermetallics: Synthesis mechanism, pore structure, and material properties. *J. Mater. Sci. Technol.* **2021**, *74*, 89–104. [[CrossRef](#)]
13. Zhong, Q.; Pan, D.; Zuo, S.; Li, X.; Luo, H.; Lin, Y. Fabrication of Mg[sbnd]Zn intermetallic layer with high hardness and corrosion resistance on AZ31 alloy. *Mater. Charact.* **2021**, *179*, 111365. [[CrossRef](#)]
14. Liu, W.; Li, L.; Lin, S.; Luo, Y.; Bao, Z.; Mao, Y.; Li, K.; Wu, D.; Peng, H. Confined Ni-In intermetallic alloy nanocatalyst with excellent coking resistance for methane dry reforming. *J. Energy Chem.* **2021**, *65*, 34–47. [[CrossRef](#)]
15. Sun, Y.; Rong, Y.; Zhao, Y.; Zhao, Y.; Hang, R.; Yao, X.; Chu, P.K. Electrochemical stability, corrosion behavior, and biological properties of Ni-Ti-O nanoporous layers anodically on NiTi alloy. *Corros. Sci.* **2021**, *179*, 109104. [[CrossRef](#)]
16. Shao, L.; Xie, G.; Liu, X.; Wu, Y.; Yu, J.; Feng, K.; Xue, W. The effect of Cu content and Ti₂Cu precipitation on the combustion behaviour and mechanism of Ti-xCu alloys. *Corros. Sci.* **2021**, *190*, 109641. [[CrossRef](#)]
17. Yu, F.; Wang, H.; Yuan, G.; Shu, X. Effect of Cu content on wear resistance and mechanical behavior of Ti-Cu binary alloys. *Appl. Phys. A* **2017**, *123*, 278. [[CrossRef](#)]
18. Kriegel, M.J.; Wetzell, M.H.; Treichel, A.; Fabrichnaya, O.; Rafaja, D. Binary Ti-Fe system. Part I: Experimental investigation at high pressure. *Calphad Comput. Coupling Phase Diagr. Thermochem.* **2021**, *74*, 102322. [[CrossRef](#)]
19. Ebrahimian, M.; Enayati, M.H.; Karimzadeh, F.; Min, Y.; Kim, D.E. Microstructure and mechanical properties of hot-pressed Ti-Co-Si compounds reinforced by intermetallic phases. *Mater. Charact.* **2021**, *171*, 110816. [[CrossRef](#)]
20. Liu, Z.; Liu, Z.; Ji, S.; Liu, Y.; Jing, Y. Fabrication of Ti-Si intermetallic compound porous membrane using an in-situ reactive sintering process. *Mater. Lett.* **2020**, *271*, 127786. [[CrossRef](#)]
21. Burkov, A.A.; Chigrin, P.G. Synthesis of Ti-Al intermetallic coatings via electrospark deposition in a mixture of Ti and Al granules technique. *Surf. Coat. Technol.* **2020**, *387*, 127786. [[CrossRef](#)]
22. Du, C.; Xiao, J.; Zhang, B.; Zhu, H. Facile synthesis of fine Ti-Al intermetallic compound powders via sodiothermic reduction in molten CaCl₂. *Intermetallics* **2021**, *129*, 107038. [[CrossRef](#)]
23. Seyyedi, A.; Abdoos, H. An examination of microstructure and dry wear properties of Nano-Y₂O₃ incorporated in fine-grained W-Ni-Cu alloy prepared by conventional and spark plasma sintering. *Int. J. Refract. Met. Hard Mater.* **2022**, *102*, 107038. [[CrossRef](#)]
24. Yaprıntseva, E.; Vasil’ev, A.; Yaprıntsev, M.; Ivanov, O. Thermoelectric properties of medium-entropy PbSbTeSe alloy prepared by reactive spark plasma sintering. *Mater. Lett.* **2022**, *309*, 131416. [[CrossRef](#)]
25. Papynov, E.K.; Shichalin, O.O.; Mayorov, V.Y.; Kuryavyi, V.G.; Kaidalova, T.A.; Teplukhina, L.V.; Portnyagin, A.S.; Slobodyuk, A.B.; Belov, A.A.; Tananaev, I.G.; et al. SPS technique for ionizing radiation source fabrication based on dense cesium-containing core. *J. Hazard. Mater.* **2019**, *369*, 25–30. [[CrossRef](#)]
26. Simonenko, T.L.; Kalinina, M.V.; Simonenko, N.P.; Simonenko, E.P.; Glumov, O.V.; Mel’nikova, N.A.; Murin, I.V.; Shichalin, O.O.; Papynov, E.K.; Shilova, O.A.; et al. Synthesis of BaCe_{0.9-x}Zr_xY_{0.1}O_{3- Δ} nanopowders and the study of proton conductors fabricated on their basis by low-temperature spark plasma sintering. *Int. J. Hydrogen Energy* **2019**, *44*, 20345–20354. [[CrossRef](#)]
27. Papynov, E.K.; Portnyagin, A.S.; Modin, E.B.; Mayorov, V.Y.; Shichalin, O.O.; Golikov, A.P.; Pechnikov, V.S.; Gridasova, E.A.; Tananaev, I.G.; Avramenko, V.A. A complex approach to assessing porous structure of structured ceramics obtained by SPS technique. *Mater. Charact.* **2018**, *145*, 294–302. [[CrossRef](#)]
28. Papynov, E.K.; Shichalin, O.O.; Mironenko, A.Y.; Ryakov, A.V.; Manakov, I.V.; Makhrov, P.V.; Buravlev, I.Y.; Tananaev, I.G.; Avramenko, V.A.; Sergienko, V.I. Synthesis of High-Density Pellets of Uranium Dioxide by Spark Plasma Sintering in Dies of Different Type. *Radiochemistry* **2018**, *60*, 362–370. [[CrossRef](#)]
29. Papynov, E.K.; Mayorov, V.Y.; Portnyagin, A.S.; Shichalin, O.O.; Koblyakov, S.P.; Kaidalova, T.A.; Nepomnyashiy, A.V.; Sokol, T.A.; Zub, Y.L.; Avramenko, V.A. Application of carbonaceous template for porous structure control of ceramic composites based on synthetic wollastonite obtained via Spark Plasma Sintering. *Ceram. Int.* **2015**, *41*, 1171–1176. [[CrossRef](#)]
30. Simonenko, E.P.; Simonenko, N.P.; Gordeev, A.N.; Papynov, E.K.; Shichalin, O.O.; Kolesnikov, A.F.; Avramenko, V.A.; Sevastyanov, V.G.; Kuznetsov, N.T. Study of the thermal behavior of wedge-shaped samples of HfB₂-45 vol % SiC ultra-high-temperature composite in a high-enthalpy air flow. *Russ. J. Inorg. Chem.* **2018**, *63*, 421–432. [[CrossRef](#)]

31. Simonenko, E.P.; Simonenko, N.P.; Gordeev, A.N.; Kolesnikov, A.F.; Papynov, E.K.; Shichalin, O.O.; Tal'skikh, K.Y.; Gridasova, E.A.; Avramenko, V.A.; Sevastyanov, V.G.; et al. Impact of a Supersonic Dissociated Air Flow on the Surface of HfB₂-30 vol % SiC UHTC Produced by the Sol-Gel Method. *Russ. J. Inorg. Chem.* **2018**, *63*, 1484–1493. [[CrossRef](#)]
32. Papynov, E.K.; Shichalin, O.O.; Buravlev, I.Y.; Portnyagin, A.S.; Belov, A.A.; Maiorov, V.Y.; Skurikhina, Y.E.; Merkulov, E.B.; Glavinskaya, V.O.; Nomerovskii, A.D.; et al. Reactive Spark Plasma Synthesis of Porous Bioceramic Wollastonite. *Russ. J. Inorg. Chem.* **2020**, *65*, 263–270. [[CrossRef](#)]
33. Dong, R.; Zhu, W.; Zhao, C.; Zhang, Y.; Ren, F. Microstructure, Mechanical Properties, and Sliding Wear Behavior of Spark Plasma Sintered Ti-Cu Alloy. *Metall. Mater. Trans. A* **2018**, *49*, 6147–6160. [[CrossRef](#)]
34. Brice, D. *An Assessment of Uncommon Titanium Binary Systems: Ti-Zn, Ti-Cu, and Ti-Sb*; University of North Texas: Denton, TX, USA, 2015.
35. Poondla, N.; Srivatsan, T.S.; Patnaik, A.; Petraroli, M. A study of the microstructure and hardness of two titanium alloys: Commercially pure and Ti-6Al-4V. *J. Alloys Compd.* **2009**, *486*, 162–167. [[CrossRef](#)]
36. Chenna, K.S.; Jha, A.J.; Bhanu, P. On the Prediction of Strength from Hardness for Copper Alloys. *J. Mater.* **2013**, *2013*, 352578.
37. *International Standard 16151*; Corrosion of Metals and Alloys—Accelerated Cyclic Test with Exposure to Acidified Salt Spray, Dry and Wet Conditions. ISO: Geneva, Switzerland, 2018.